*Progress In Electromagnetics Research Letters, Vol. 104, 57–65, 2022*

# A Circular Slotted Shaped UWB Monopole Antenna for Breast Cancer Detection

**Venkata L. N. Phani Ponnapalli[1, *], Shanumugam Karthikeyan[1], and Jammula L. Narayana[2]**

**Abstract**—The design of an innovative breast model system that focuses on a wideband for the detection of malignant tumours is described. The planned antenna has an overall area of $18 \times 28\,\text{mm}^2$ and a fractional bandwidth (FBW) of 99% across a frequency spectrum of 3.4–10 GHz. The suggested antenna has excellent impedance matching, a considerable gain of 3.95 dBi, maximum efficiency of 96.98%. Omnidirectional radiated patterns are verified in the frequency, and time-domain analysis is also investigated for breast tumor diagnosis. For detecting a breast tumor with accuracy, the suggested antenna $S_{21}$ parameters are evaluated together, including imaging outcomes of current densities and specific absorption rate (SAR). These findings show that the radiator and the whole system work well at finding the tumor.

## 1. INTRODUCTION

Many improvements over existing imaging modalities like computed tomography (CT) and X-ray radiography have emerged in the past few years for investigation on microwave imaging (MI). Female breast cancer is the leading cause of malignancy in developed nations [1]. Early diagnosis of breast cancer is believed to improve treatment outcomes. Microwave imaging system (MIS) allows for a detailed investigation of breast tissues. It assists in determining morphological alterations in these tissues. The forthcoming ultra-wideband (UWB) MI promises excellent outcomes because of its non-ionizing signals operating at hundreds of MHz and tens of GHz. Antennas are vital in developing a sensor network in these systems. Because the instrument is so close to the human body, optimization is critical. Microwave imaging has been getting a lot of attention because it can help doctors find and place cancerous tissue in the female breast [2–5]. Microwave imaging systems are regarded as an option in contrast to X-ray mammography owing to their low cost and few side effects. MI uses extremely low levels of microwave radiation to image the breast tissue. The electrical characteristics of benign and diseased breast tissue vary, allowing tumor identification and localization. Because a cancerous tumor includes so much more water and blood than normal breast tissue, it scatters microwave signals more than normal. As shown in Figure 1 [6], a linear array can be used to get this scattered signal and process it on a computer. When it comes to identifying malignant tissue, there are two ways that are often employed. The first one is by using microwave tomography [7] to solve forward and backward electromagnetic field issues that can be hard to figure out in a woman's breasts. Each of these problems can be solved with a single frequency, but a multi-frequency method makes it easier to find [8]. Another way to look at things is to use microwave imaging, which is when users send and receive short pulses at different places on a probe radiator or array elements [9]. These are then concatenated to produce a two-or three-dimensional picture revealing the locations of highly reflective items bearing malignant tissue [10]. Multiple-frequency tomography and radar necessitate UWB antenna elements,

*Received 2 April 2022, Accepted 11 May 2022, Scheduled 24 May 2022*

* Corresponding author: Venkata Lakshmi Narayana Phani Ponnapalli (pvlnphani0454@gmail.com).

[1] Department of ECE, Annamalai University, Chidambaram, T.N, India. [2] Department of ECE, PSCMR College of Engineering & Technology, Vijayawada, A.P, India.

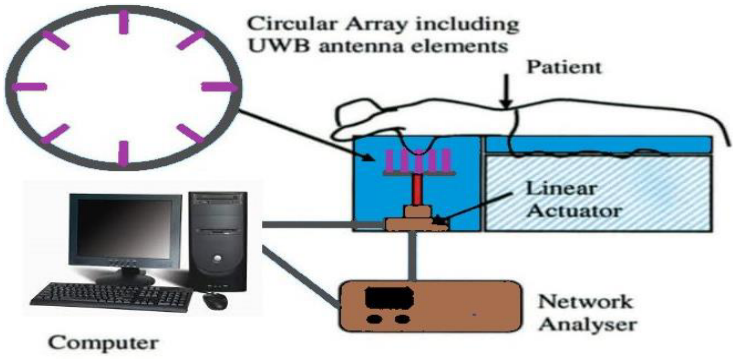


**Figure 1.** Microwave imaging (MI) system for breast tumor diagnosis.

especially planar. Many UWB element layouts have already been proposed in the context of UWB communications. The majority of these antennas are planar monopoles with rectangular, circular, and elliptical designs [11–13]. The current designs of these antennas do not make them easy to use for microwave imaging. The reasons are as follows: UWB planar monopoles with an omnidirectional radiation pattern and low gain are often used in communication applications with UWB communication. The dynamic range is diminished if they are used in a microwave image sensor. It is intended as a circular slotted antenna formed of a high dielectric constant substrate material to lessen the antenna's size, overcoming the previous disadvantages. The radiation efficiency rises 90% with the rather high gain for such a low loss over the targeted band.

### 1.1. The Function of UWB in MI

The UWB MI approach needs to send and receive shorter pulses for different antenna areas or array antennas. So, it demands the use of a UWB transmitter and receiver to construct microwave radar. Thus, UWB antenna sensors play an essential part in microwave imaging systems (MISs). They also need a wider bandwidth to make a high-resolution picture [14] and to keep short-duration pulses to minimise distortion [15]. In MIS, the radiator functions as both a transmitting and receiving sensor. The transmitter element distributes microwave radiation through the breast tissue, while the reception antenna picks up scattered signals from the target and sends them back to the antenna. Various researches [16–18] show that a single-order UWB antenna may provide an astonishing tradeoff between increased resolution imaging and profound tissue penetration.

Thus, the present work is focused on the development of low-profile, easy setup, and high concert UWB antennas that can be used in MI breast tumor diagnosis. The paper is divided into five sections. Radiator design and the step-by-step design process are described in Section 2. The suggested UWB antenna's simulations and measurement results are discussed in Section 3. The imaging abilities of the antenna that will be used to image for cancerous tissue in the breast phantom is discussed in Section 4. The conclusions are presented in Section 5.

## 2. ANTENNA DESIGN METHODOLOGY

The optimized design and step-by-step implementation of ground and patch structures of the proposed antenna and their $S$-parameters are discussed in this section.

### 2.1. Antenna Design

The designed radiator in Figure 2 is etched on an FR-4 substrate with 4.3 relative permittivity, 0.002 loss tangent, 1.6 mm thickness, and $W_S \times L_S\,\text{mm}^2$ dimension. It is fed via a $50\,\Omega$ strip line with a width and length of $W_F$ and $L_F$, respectively. The patch structure of the proposed element consists of a notched circular structure and a modified rectangular ground structure that is etched below the substrate. Optimised dimensional values of proposed antenna are obtained by performing parametric

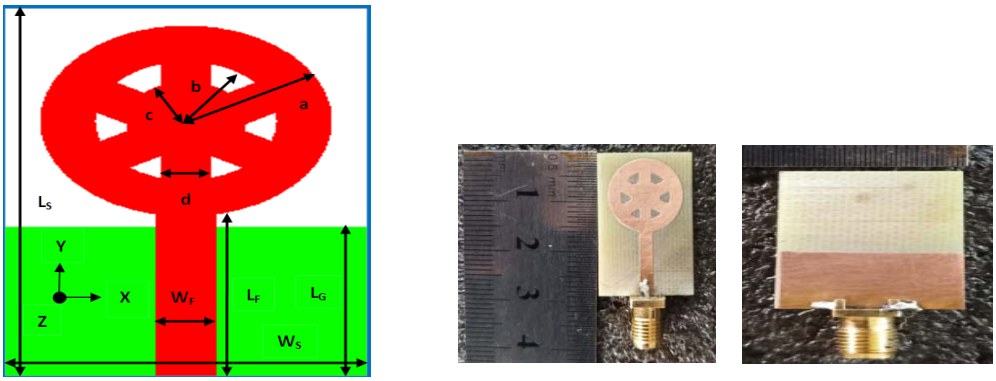


(a) (b)

**Figure 2.** Proposed antenna. (a) Dimensions. (b) Prototype.

analysis of various antenna parameters like width ($W_S$) and length ($L_G$) of the defected ground structure, radii $(a, b, c)$ of the slots of the patch and to match $50\,\Omega$ microstrip feed line with the proposed patch structure, and the width of feed ($W_F$) and length of the feed ($L_F$) are optimized by using CST Microwave studio ver.2021. The optimum antenna dimensions are: $W_S = 18\,\text{mm}$, $L_S = 28\,\text{mm}$, $W_F = 3\,\text{mm}$, $L_F = 15.5\,\text{mm}$, $L_G = 11.5\,\text{mm}$, $a = 7.25\,\text{mm}$, $b = 4.5\,\text{mm}$, $c = 3\,\text{mm}$, $d = 2.5\,\text{mm}$.

### 2.2. Implementation of Proposed Antenna

The design approach of intended patch structure is illustrated in Figure 3, and the $S_{11}$ parameters are shown in Figure 4. Initially, in the first stage a circular ring of radii $b$ is etched from a circle of radii $a$, and then it is embedded with a $50\,\Omega$ line along with full ground to obtain the antenna structure Ant$\Psi$1. The antenna structure, Ant$\Psi$1, does not provide any resonances as shown in Figure 4. In the second stage, Ant$\Psi$2 is achieved by notching a rectangular defected ground structure to achieve a $-10\,\text{dB}$ impedance bandwidths span of 3.35–4.82 GHz and 8.2–9.37 GHz with resonances occurring at 3.81 GHz and 8.85 GHz having the peak $S_{11}$ values of $-18.06\,\text{dB}$ and $-11.40\,\text{dB}$, respectively. In the third stage, a single resonance occurs at 3.8 GHz to cover an impedance bandwidth of 3.34–4.85 GHz with a peak $S_{11}$ of $-18.56\,\text{dB}$, by inserting a circle in the slotted patch structure of Ant$\Psi$2 to obtain Ant$\Psi$3. Finally, the proposed antenna structure Ant$\Psi$4 is obtained by inserting three rectangular patches connecting the inner and outer circles of the antenna structure Ant$\Psi$3 to cover a UWB bandwidth of 3.4–10 GHz with two resonances at 3.96 GHz and 8.67 GHz with peak $S_{11}$ values of $-16.14\,\text{dB}$ and $-22.54\,\text{dB}$ as depicted in Figure 4.

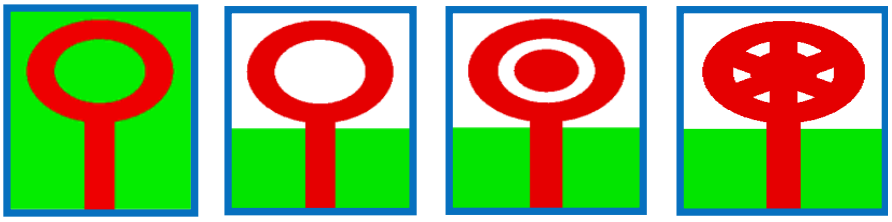

(a) (b) (c) (d)

**Figure 3.** Design process of proposed radiator. (a) Ant$\Psi$1, (b) Ant$\Psi$2, (c) Ant$\Psi$3, (d) Ant$\Psi$4.

## 3. RESULTS AND DISCUSSIONS

This section describes the insights about the modelling and measurement conclusions of the developed radiator. A photolithographic etching process is used to make the antenna, which is then tested for $S_{11}$, gain, efficiency, and radiation pattern.

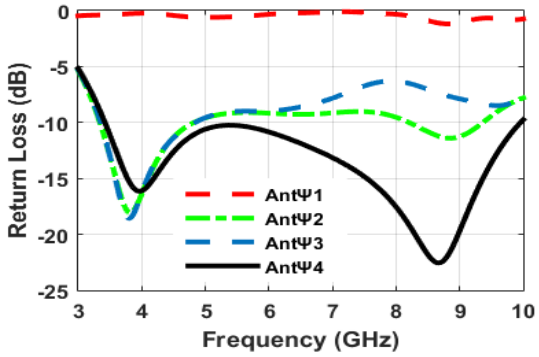


**Figure 4.** $S$-parameters of proposed antenna in different stages.

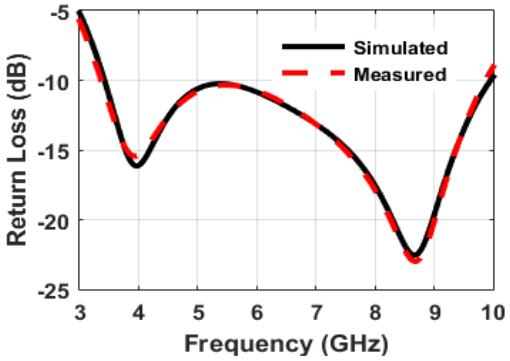


**Figure 5.** Simulated and measured return loss ($S_{11}$).

### 3.1. Simulated and Measured $S_{11}$

For UWB MI, the radiator bandwidth must have an $S_{11} < -10$ dB over the entire frequency range [14]. A Vector Network Analyzer (VNA) measures $S_{11}$ on the prototype, and the results are shown in Figure 5. The findings are compared to the simulated outcomes. In simulation and measurement, $S_{11}$ is less than $-10$ dB over a 3.4–10 GHz and 3.38–9.92 GHz bandwidth, respectively, demonstrating that the designed and constructed antenna provides excellent impedance matching for the entire UWB spectrum. The antenna construction process, testing cable of the vector network analyser (VNA), and solder of the SMA connector are all potential causes of the little deviation in operational frequency bands noticed. The developed antenna's higher bandwidth fulfils the criteria for breast cancer detection with optimal resolution, with lower frequencies needed for deeper penetration.

### 3.2. Gain and Efficiency

A moderate gain antenna is suitable for sensor systems, such as UWB MI systems for breast cancer diagnosis [19]. Figure 6(a) illustrates the proposed antenna's peak gain vs frequency. As shown in the graph, the gain ranges 2.04–3.95 dBi, with a median gain of 3.07 dBi. The radiator has a high gain of 3.95 dBi at 5.8 GHz, which means that it is a feasible choice for cancer detection. As seen in Figure 6(b), the antenna's simulation and experimental efficiency are shown. The maximum efficiency of 96.98% and an average efficiency of around 90.21% might well be noted across the operational bandwidth.

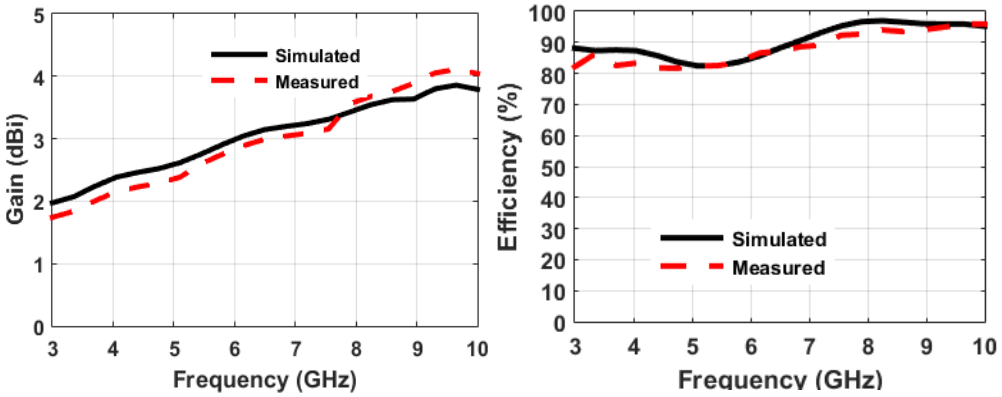


**Figure 6.** Simulated and measured (a) gain, (b) efficiency.

### 3.3. Simulated and Measured Radiation Patterns

Figure 7 depicts the intended antenna's simulated and observed patterns. The $E$-plane radiation pattern of the UWB slot antenna is dipole-shaped, whereas the $H$-plane pattern is omnidirectional. The measured patterns are quite similar to the simulated ones, although some slight variations may be explained by the testing and modelling settings.

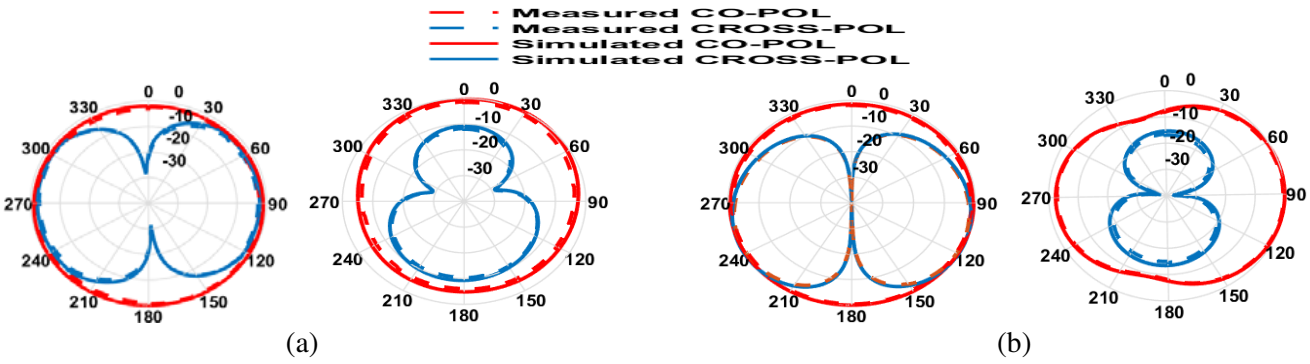


**Figure 7.** Simulated and measured radiation patterns. (a) 3.96 GHz, (b) 8.67 GHz.

## 4. IMAGING RESULTS AND DISCUSSION

A prototype was developed and tested in order to verify the simulated results. Breast cancer imaging systems need to have antennas that are close to the breast in order to get the best results. Consequently, the influence of breast tissue on the antenna's performance is examined. This section will present the dielectric characteristics of human tissues, which are required to comprehend quantitative microwave imaging. Figure 8(a) shows a breast phantom that can be used to simulate and test the detection of breast tumors. The phantom comprises three layers: skin, fat, and breast tumor. The dielectric constant is 36.7, the electrical conductivity 2.34 S/m, and the density 1,109 kg/m$^3$ in the outermost skin layer. Fat has a dielectric constant of 4.84, a conductivity of 0.262 S/m, and a density of 911 kg/m$^3$. The breast tumor has an electrical conductivity of 4 S/m, a dielectric constant of 54.9, and a density of 1058 kg/m$^3$.

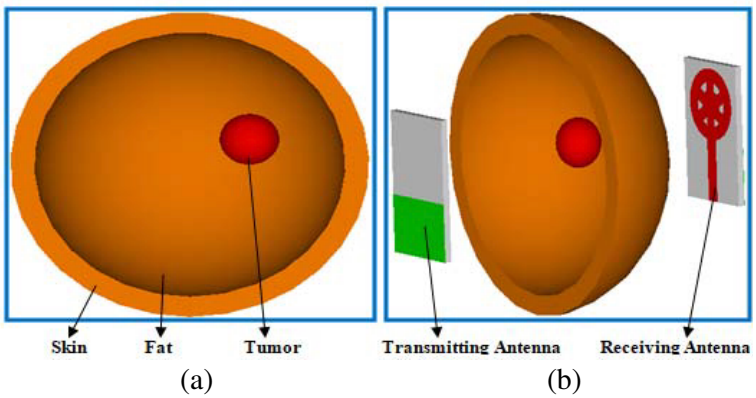


**Figure 8.** (a) Breast phantom. (b) Simulation setup for breast cancer imaging.

According to the variations in complex permittivity, the dielectric characteristics of nonmetallic materials are evaluated in biological applications in quantitative microwave imaging, defined by [20],

$$\varepsilon^* = \varepsilon' - j\varepsilon'' \tag{1}$$

where $\varepsilon'$ is the relative permittivity detailing the polarization impact of charged particles in the tissue and $\varepsilon''$ expressing the out-of-phase losses cause of the displacement currents produced by the used electromagnetic field. Table 1 depicts the electrical behavior of the skin, fat, and tumor.

**Table 1.** Dielectric properties for the different tissue types found in the breast.

| Tissues | Conductivity, S/m | Density, kg/m$^3$ | dielectric constant, $\varepsilon$ |
|---|---|---|---|
| Skin | 2.34 | 1109 | 36.7 |
| Fat | 0.262 | 911 | 4.84 |
| Tumor (malignant) | 4 | 1058 | 54.9 |

A breast phantom is employed to model the results of the designed microwave imaging system in CST as stated in Figure 8(b) to better understand the system. In the direction of the breast phantom, two antennas are mounted, 300 mm apart. One is a transmitter, while the other is a receiver in this case. There are differences in received signals throughout the breast phantom because of the dielectric characteristics of breast and tumor tissue.

When a narrow pulse is to be sent from one element, the received pulse is estimated and shown in Figures 9(a) and 9(b) in side-by-side and face-to-face combinations. The stimulated and received pulses are normalised to their peaks. Thus, the antenna that was designed can operate in a distortion-free narrow pulse mode, which makes it ideal for microwave imaging. An array of elements surrounds the breast in the imaging system that will be employed with the antenna. As a result, it is critical to analyse the value of mutual coupling among these antennas. Figure 10 illustrates the proposed antenna's $S$-parameters. As depicted in Figure 8(b), the simulation setting of the described antennas around the

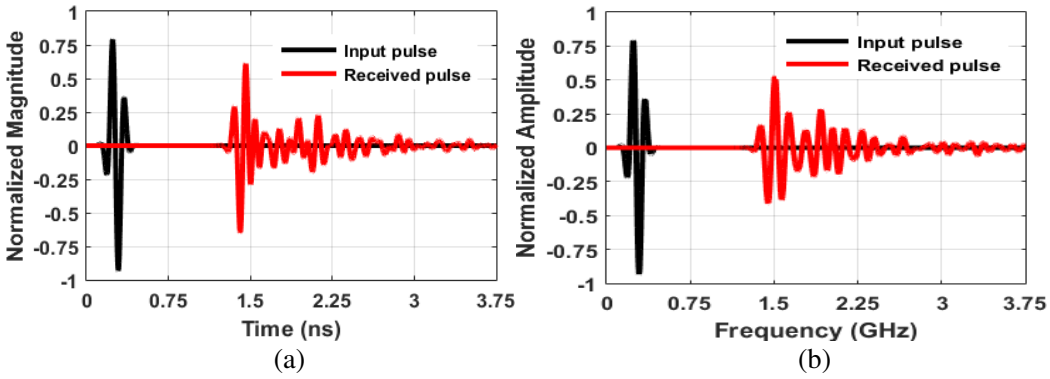


**Figure 9.** Normalized input and output pulses. (a) Side-by-side. (b) Face-to-face.

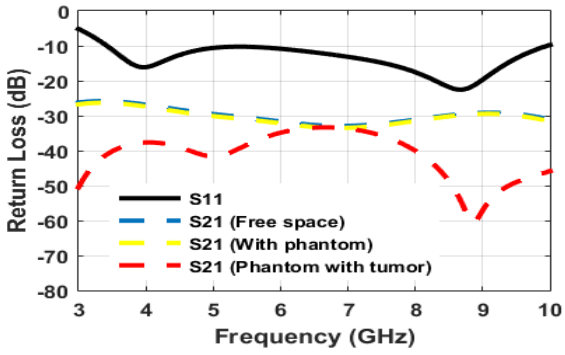


**Figure 10.** $S$-parameters of the imaging set up.

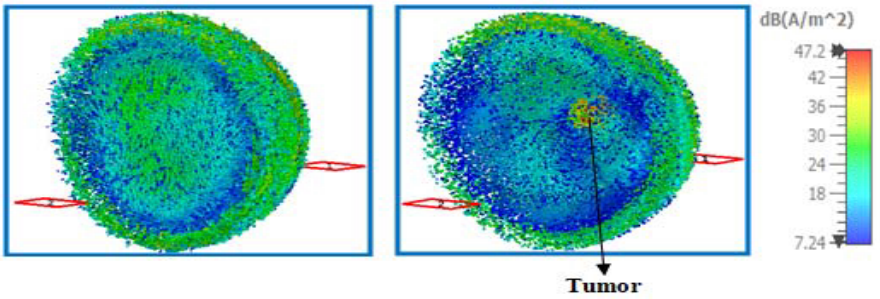


**Figure 11.** Current desnsities for (a) healthy, (b) malignant tumor.

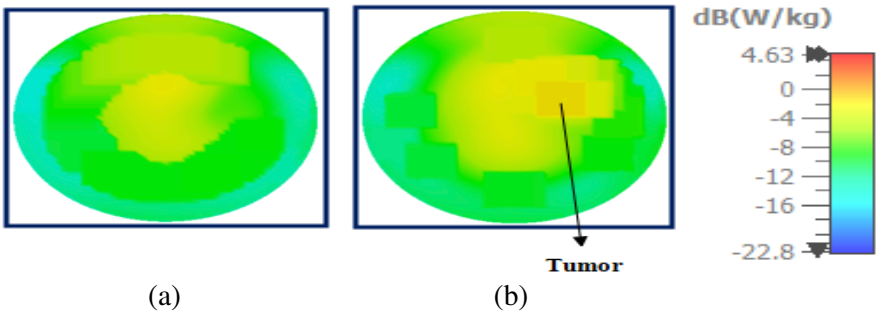


**Figure 12.** SAR Imaging results for (a) healthy, (b) malignant tumor.

breast phantom was used to be face-to-face with a distance of 300 mm to estimate the $S$-parameters of the suggested antenna. To assess the performance of the antenna elements, we evaluate $S_{11}$ and $S_{21}$ correlation in three distinct scenarios: free space, only with breast phantom and breast phantom with tumor are illustrated in Figure 10. The antenna covers 3.4 to 10 GHz. A considerable difference can be shown in Figure 10, between the $S_{21}$ result in free space only with the breast phantom and the breast phantom with tumor in between the transmitting and receiving antennas, respectively. Image findings for the proposed antenna's current density and specific absorption rate (SAR) at 8.81 GHz are shown in Figure 11 and Figure 12. Healthy breast tissue imaging findings without tumours are shown in blue and green color scales in Figures 11(a) and 12(a). Figure 11(b) and Figure 12(b) show the absolute position

**Table 2.** Comparison of proposed radiator with reported literature.

| Ref. | Size ($mm^2$) | Electrical size | Area ($mm^2$) | B.W (GHz) | R.E (%) | Microwave Imaging |
|---|---|---|---|---|---|---|
| [21] | $20 \times 28$ | $0.20\lambda_0 \times 0.27\lambda_0$ | 560 | 2.95–12 | NR | Reported |
| [19] | $35 \times 20$ | $0.31\lambda_0 \times 0.32\lambda_0$ | 700 | 3–12 | NR | Reported |
| [22] | $30 \times 35$ | $0.31\lambda_0 \times 0.26\lambda_0$ | 1050 | 2.04–14.6 | NR | NR |
| [23] | $30 \times 30$ | $0.40\lambda_0 \times 0.40\lambda_0$ | 900 | 4–18 | NR | Reported |
| [24] | $30 \times 32.5$ | $0.27\lambda_0 \times 0.29\lambda_0$ | 975 | 2.73–11 | NR | NR |
| [25] | $32 \times 32$ | $0.5\lambda_0 \times 0.5\lambda_0$ | 1024 | 4.68–11.8 | NR | Reported |
| [26] | $45 \times 40$ | $0.35\lambda_0 \times 0.31\lambda_0$ | 1800 | 2.36–14.6 | NR | Reported |
| **Prop** | **$18 \times 28$** | **$0.20\lambda_0 \times 0.31\lambda_0$** | **504** | **3.4–10** | **96.98** | **Reported** |

NR: Not Reported, R.E: Radiation Efficiency, $\lambda_0$: Wavelength at lower frequency.

of the tumor in the breast phantom by the red color concentrations both for current densities and SAR plots. The images demonstrate that high-resolution imaging can establish the tumor's location and existence.

As a conclusion, the findings of microwave breast phantom images show that the antenna's features are adequate for microwave imaging applications. The comparisons of size and radiation performance of the proposed antenna with similar reported antennas reported in literature are illustrated in Table 2.

## 5. CONCLUSION

This article describes a small UWB planar radiator with a circular slotted patch and a rectangular DGS. The antenna's overall dimensions are $18 \times 28\,\text{mm}^2$, and it has a broad impedance bandwidth of 6.6 GHz (3.4–10 GHz) with a significant gain of 3.95 dBi, high radiation efficiency of 96.98%, and consistent radiation patterns. In order to show that the radiator is good for MI, its frequency and time-domain properties are measured and analyzed. The proposed antenna successfully diagnoses the tumor inside the breast-phantom by analysing a simulation environment with the breast-phantom. The low profile, compact size, high bandwidth, and imaging results of the proposed radiator make it appropriate for microwave breast imaging.

## REFERENCES

1. Raghavan, S. and M. Ramaraj, "An overview of microwave imaging towards for breast cancer diagnosis," *Progress In Electromagnetics Research Symposium Proceedings*, 627–630, Moscow, Russia, Aug. 19–23, 2012.
2. Jayant, S., G. Srivastava, and R. Purwar, "Bending and SAR analysis on UWB wearable MIMO antenna for on-arm WBAN applications," *Frequenz*, Vol. 75, Nos. 5–6, 177–189, 2021.
3. Kanj, H. and M. Popovic, "A novel ultra-compact broadband antenna for microwave breast tumor detection," *Progress In Electromagnetics Research*, Vol. 86, 169–198, 2008.
4. Kaabal, A., M. El halaoui, S. Ahyoud, and A. Asselman, "Dual band-notched WiMAX/WLAN of a compact ultrawideband antenna with spectral and time-domains analysis for breast cancer detection," *Progress In Electromagnetics Research C*, Vol. 65, 163–173, 2016.
5. Salvador, S. M. and G. Vecchi, "Experimental tests of microwave breast cancer detection on phantoms," *IEEE Transactions on Antennas and Propagation*, Vol. 57, No. 6, 1705–1712, 2009.
6. Abbosh, A. M., H. K. Kan, and M. E. Bialkowski, "Compact ultra-wideband planar tapered slot antenna for use in a microwave imaging system," *Microwave and Optical Technology Letters*, Vol. 48, No. 11, 2212–2216, 2006.
7. Meaney, P. M., K. D. Paulsen, J. T. Chang, M. W. Fanning, and A. Hartov, "Nonactive antenna compensation for fixed-array microwave imaging," *IEEE Transactions on Medical Imaging*, Vol. 18, No. 6, 496–507, 1999.
8. Fang, Q., "Computational methods for microwave medical imaging," PhD Thesis, Thayer School of Engineering, Dartmouth College, Hanover, New Hampshire, NH, Dec. 2004.
9. Bond, E. J., X. Li, S. C. Hagness, and B. D. van Veen, "Microwave imaging via space-time beam forming for early detection of breast cancer," *IEEE Transactions on Antennas and Propagation*, Vol. 51, No. 8, 1690–1705, 2003.
10. Bialkowski, M. E., W. C. Khor, and S. Crozier, "A planar microwave imaging system with step-frequency synthesized pulse using different calibration methods," *Microwave and Optical Technology Letters*, Vol. 48, No. 3, 511–516, 2006.
11. Rao Devana, V. N. K. and A. Maheswara Rao, "Compact UWB monopole antenna with quadruple band notched characteristics," *International Journal of Electronics*, Vol. 107, No. 2, 175–196, 2020.
12. Rao Devana, V. N. K. and A. Maheswara Rao, "A novel fan shaped UWB antenna with band notch for WLAN using a simple parasitic slit," *International Journal of Electronics Letters*, Vol. 7, No. 3, 352–366, 2019.

13. Rao Devana, V. N. K. and A. Maheswara Rao, "Design and analysis of dual band notched UWB antenna using a slot in feed and asymmetrical parasitic," *IETE Journal of Research*, 2020, doi: 10.1080/03772063.2020.1816226.
14. Afifi, A.I., A. B. Abdel-Rahman, A. Allam, and A. A. El-Hameed, "A compact ultra-wideband monopole antenna for breast cancer detection," *2016 IEEE 59th International Midwest Symposium on Circuits and Systems (MWSCAS)*, 1–4, IEEE, 2016.
15. Molaei, A., M. Kaboli, S. A. Mirtaheri, and M. S. Abrishamian, "Dielectric lens balanced antipodal Vivaldi antenna with low cross-polarisation for ultra-wideband applications," *IET Microwaves, Antennas & Propagation*, Vol. 8, No. 14, 1137–1142, 2014.
16. Bakar, A. A., D. Ireland, A. M. Abbosh, and Y. Wang, "Experimental assessment of microwave diagnostic tool for ultra-wideband breast cancer detection," *Progress In Electromagnetics Research M*, Vol. 23, 109–121, 2012.
17. Latif, S., D. Flores-Tapia, S. Pistorius, and L. Shafai, "A planar ultrawideband elliptical monopole antenna with reflector for breast microwave imaging," *Microwave and Optical Technology Letters*, Vol. 56, No. 4, 808–813, 2014.
18. Jalilvand, M., X. Li, L. Zwirello, and T. Zwick, "Ultra wideband compact near-field imaging system for breast cancer detection," *IET Microwaves, Antennas & Propagation*, Vol. 9, No. 10, 1009–1014, 2015.
19. Amdaouch, I., O. Aghzout, A. Naghar, A. V. Alejos, and F. J. Falcone, "Breast tumor detection system based on a compact UWB antenna design," *Progress In Electromagnetics Research M*, Vol. 64, 123–133, 2018.
20. Tarikul Islam, M., M. Samsuzzaman, M. N. Rahman, and M. T. Islam, "A compact slotted patch antenna for breast tumor detection," *Microwave and Optical Technology Letters*, Vol. 60, No. 7, 1600–1608, 2018.
21. Lasemi, Z. and Z. Atlasbaf, "Impact of fidelity factor on breast cancer detection," *IEEE Antennas and Wireless Propagation Letters*, Vol. 19, No. 10, 1649–1653, 2020.
22. Rao Devana, V. N. K., B. S. L. Mounika, B. Yamini, G. Anitha, and G. Bala Sai Tarun, "Novel UWB monopole antenna with band notched characteristics," *International Journal of Signal Processing, Image Processing and Pattern Recognition*, Vol. 9, No. 5, 291–296, 2016.
23. Gupta, A. and M. L. Meena, "Design of semi circular floral shape directive UWB antenna for radar based microwave imaging," *2021 International Conference on Intelligence and Smart Systems (ICAIS)*, 2021, doi: 10.1109/ICAIS50930.2021.9395839.
24. Rao Devana, V. N. and A. M. Rao, "Design and parametric analysis of beveled UWB triple band rejection antenna," *Progress In Electromagnetics Research M*, Vol. 84, 95–106, 2019.
25. Zhang, H. and H. Li, "Flexible dual-polarized UWB antennas for breast tumor imaging," *2020 IEEE MTT-S International Conference on Numerical Electromagnetic and Multiphysics Modeling and Optimization (NEMO)*, 2020, doi: 10.1109/NEMO49486.2020.9343495.
26. Akazzim, Y., M. Kanjaa, O. El Mrabet, L. Jofre, and M. Essaaidi, "An UWB tapered slot vivaldi antenna (TSA) with improved characteristics," *2019 IEEE 19th Mediterranean Microwave Symposium (MMS)*, 2019, doi: 10.1109/MMS48040.2019.9157265.